Radial carpet beams: A class of nondiffracting, accelerating, and self-healing beams

Saifollah Rasouli*
Department of Physics, Institute for Advanced Studies in Basic Sciences (IASBS), Zanjan 45137-66731, Iran and Optics Research Center, Institute for Advanced Studies in Basic Sciences (IASBS), Zanjan 45137-66731, Iran

Ali Mohammad Khazaei and Davud Hebri
Department of Physics, Institute for Advanced Studies in Basic Sciences (IASBS), Zanjan 45137-66731, Iran

(Received 23 January 2018; published 23 March 2018)

Self-accelerating shape-invariant beams are attracting major attention, presenting applications in many areas such as laser manipulation and patterning, light-sheet microscopy, and plasma channels. Moreover, optical lattices are offering many applications, including quantum computation, quantum phase transition, spin-exchange interaction, and realization of magnetic fields. We report observation of a class of accelerating and self-healing beams which covers the features required by all the aforementioned applications. These beams are accelerating, shape invariant, and self-healing for more than several tens of meters, have numerous phase anomalies and unprecedented patterns, and can be feasibly tuned. Diffraction of a plane wave from radial phase gratings generates such beams, and due to their beauty and structural complexity we have called them "carpet" beams. By tuning the value of phase variations over the grating, the resulting carpet patterns are converted into two-dimensional optical lattices with polar symmetry. Furthermore, the number of spokes in the radial grating, phase variation amplitude, and wavelength of the impinging light beam can also be adjusted to obtain additional features. We believe that radial carpet beams and lattices might find more applications in optical micromanipulation, optical lithography, super-resolution imaging, lighting design, optical communication through atmosphere, etc.

DOI: 10.1103/PhysRevA.97.033844

I. INTRODUCTION

Producing optical patterns and using them has garnered a great deal of attention in optics for about four centuries. The simplest optical pattern is generated through the interference of two coherent beams. Another easy way to produce optical patterns is the use of diffraction. One of the fantastic ways of producing more complex optical patterns is using the Talbot effect. Also, the use of spatial light modulators (SLMs) is another possibility to produce more complicated optical patterns. In addition to the linear methods of generating optical patterns, there are nonlinear light-matter interaction mechanisms such as the nonlinear wave mixing in which self-generating optical patterns can be produced [1]. Optical pattern engineering and architecture for various purposes, such as producing multifocus beams for multitrapping, have received considerable attention in recent years. There are many applications for optical patterns, for example, interference patterns are used for producing periodic structures via photomicrography.

The change of the shape of conventional structured light patterns under propagation has imposed strict limits on using them in different propagation distances [2]. There are a number of nonspreading or nondiffracting beams such as Bessel [3], Airy [4,5], Mathieu [6], Weber [7], and Pearcey [8] beams that can be used at different propagation distances for various applications. It is worth remembering that the use of the Talbot effect is another way to overcome the spreading effect of diffraction [9–11]. Almost all nondiffracting beams have other interesting properties, such as self-healing [8,12], self-channeling [13], having phase anomalies [14–16], accelerating [5,7,17,18], and so on. Here, we produce a class of accelerating nondiffracting beams which have phase anomalies and are able to form a two-dimensional (2D) optical lattice with symmetry in the polar system.

In this work, a detailed theory of diffraction from radial phase gratings with sinusoidal or binary transmission functions is presented. We show that unprecedented optical carpets are produced at the transverse plane in the diffraction of a plane wave from radial phase gratings. The optical carpets produced can be easily turned into 2D optical lattices with polar symmetry by tuning the phase amplitude of the gratings. The generated lattices are characterized in terms of the radial grating spoke number, amplitude of the phase variation over the grating, and wavelength of the impinging light beam at various propagation distances.

We show that the form of the resulting lattice does not change in propagation, but each intensity spot on the lattice propagates on a curved path. These optical carpets and 2D lattices have self-healing properties. The light-beam phase distribution over the transverse plane has numerous phase anomalies. We believe that these kinds of optical lattices might find more applications in optical trapping, beam shaping, optical lithography, etc.

It is worth mentioning that we have recently reported the observation of the Talbot carpet at the transverse plane produced by the diffraction of a plane wave from an amplitude radial grating [19]. We have shown that for an amplitude radial grating, the geometric shadow and near-field and far-field diffraction patterns are observable at planes parallel to the

*Corresponding author: rasouli@iasbs.ac.ir

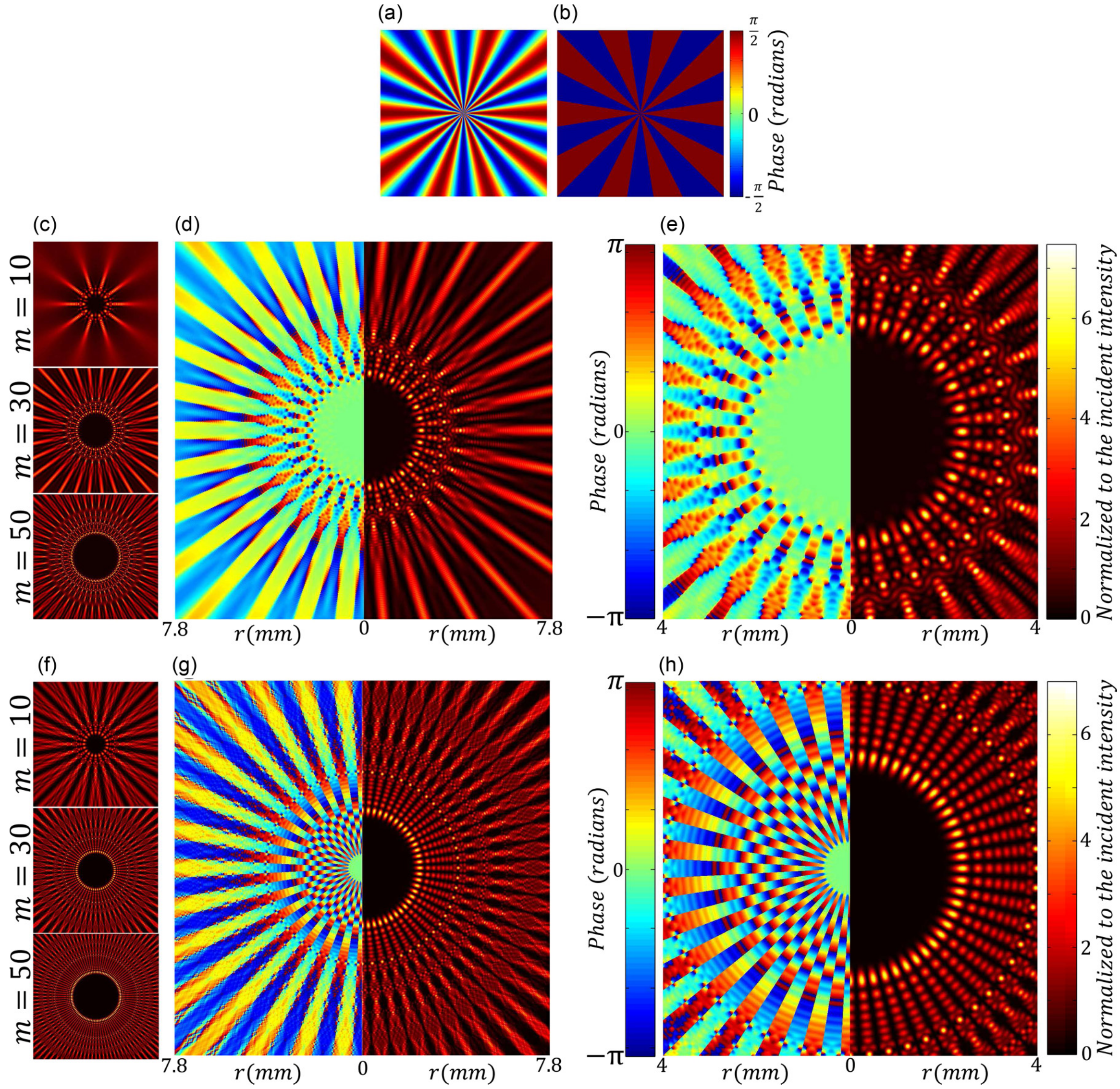

FIG. 1. Radial phase gratings and theoretically predicted optical carpets in the diffraction of a plane wave from radial phase gratings with sinusoidal and binary profiles. (a, b) Illustration of radial phase gratings with sinusoidal and binary transmission functions, respectively. Both patterns have the same number of spokes, $m = 10$. (c) Calculated diffraction patterns for three radial phase gratings having sinusoidal profiles with $m = 10$, $m = 30$, and $m = 50$ spokes at a distance 100 cm from the gratings. (d) Enlarged phase (left) and intensity (right) patterns for the grating with $m = 30$. (e) An inset of (d). (f–h) Corresponding patterns for phase gratings with binary profiles. The grating parameters are the same as (c–e). The amplitude of the phase modulation for all of the gratings is $\gamma = \pi/2$. Real size of the patterns is 15.6 mm $\times$ 15.6 mm (see also Movies 1a–1d).

grating plane and are continuous at distances from the grating. As a consequence of turning a conventional grating into a radial grating with a central singularity, it was shown that the plane boundaries between the optical regimes have acquired curvature. In another work, an intensity-based method for measuring alteration of the topological charge by the aid of diffraction of vortex beams from amplitude sinusoidal radial gratings was recently reported [20]. Also, the propagation of azimuthally periodic light fields produced by the aid of petal patterns was used for generating azimuthally modulated circular superlinear Airy beams [21]. That work is based on the diffraction of truncated circular Airy beams having an azimuthal phase periodicity. As the initial complex amplitude of the diffracted beam has a base structure including an Airy function, this limits the variety of the resulting patterns.

In the following sections, we present detailed analytical, computer simulation, and experimental works of the diffraction of a plane wave from radial phase gratings having sinusoidal and binary profiles by using the Fresnel-Kirchhoff integral. Theoretical calculations are done in the polar coordinates. The resulting diffraction patterns by each of the mentioned ways are similar and they verify each other.

II. DIFFRACTION FROM RADIAL STRUCTURES

Here, the theory of diffraction from radial structures is briefly reviewed. A structure is defined as a radial structure when there is not radial dependency in its transmission function [19]. We use (r,θ) for the polar coordinates. The transmission function of a radial structure, $t(\theta)$, can be written by

$$t(\theta) = \sum_{n=-\infty}^{+\infty} t_n e^{in\theta} = t_0 + \sum_{n=1}^{+\infty} (t_n\, e^{in\theta} + t_{-n} e^{-in\theta}), \quad (1)$$

where t_n is the nth Fourier series coefficient. By passing a coherent plane wave through this structure, the complex amplitude of the diffracted light beam after a propagation length of z can be written as [19]

$$\psi(r,\theta;z) = e^{ikz}\left\{ t_0 + \mathcal{R}e^{i\mathcal{R}^2} \sum_{n=1}^{+\infty} \sqrt{\frac{\pi}{2}}(-i)^{\frac{n}{2}+1}(t_n e^{in\theta} \right.$$
$$\left. + t_{-n}e^{-in\theta})\Big[J_{\frac{n+1}{2}}(\mathcal{R}^2) + i\,J_{\frac{n-1}{2}}(\mathcal{R}^2)\Big]\right\}, \quad (2)$$

where $k = \frac{2\pi}{\lambda}$ is the wave number, $J_{\frac{n\pm1}{2}}$ is the $\frac{n\pm1}{2}$th Bessel function of the first kind, and $\mathcal{R}$ is a dimensionless quantity determined by $\mathcal{R} = \sqrt{\frac{\pi}{2\lambda z}}r$.

The diffraction from 2D radial structures can be calculated by Eq. (2). In the following, we calculate diffraction of plane waves from radial phase gratings having sinusoidal and binary profiles.

III. DIFFRACTION OF A PLANE WAVE FROM A RADIAL PHASE GRATING HAVING A SINUSOIDAL PROFILE

Here, we present the diffraction of a plane wave from a radial phase grating with a sinusoidal profile, which is illustrated in Fig. 1(a). The grating's transmission function can be written by

$$t(\theta) = e^{i\gamma\cos(m\theta)} = \sum_{q=-\infty}^{+\infty} (i)^q J_q(\gamma) e^{iqm\theta}, \quad (3)$$

where γ and m are the amplitude of the phase variation and the number of spokes of the grating, respectively, and the Jacobi-Anger expansion is used [22]. By using $J_{-n}(x) = (-1)^n J_n(x)$ we can rewrite $t(\theta)$ as

$$t(\theta) = J_0(\gamma) + \sum_{q=1}^{+\infty}(i)^q J_q(\gamma)[e^{iqm\theta} + e^{-iqm\theta}]. \quad (4)$$

Comparing Eqs. (4) and (1), one can deduce that $t_0 = J_0(\gamma)$, $t_{n=mq} = t_{n=-mq} = (i)^q J_q(\gamma)$, $q = 1,2,3,\ldots$, and all other coefficients are zero. By using these coefficients in Eq. (2), the complex amplitude at z is given by

$$\psi(r,\theta;z) = e^{ikz}\left\{ J_0(\gamma) + \mathcal{R}e^{i\mathcal{R}^2} \times \sum_{q=1}^{+\infty} \psi_q \Big[J_{\frac{qm+1}{2}}(\mathcal{R}^2) \right.$$
$$\left. + i\,J_{\frac{qm-1}{2}}(\mathcal{R}^2)\Big]\cos(qm\theta)\right\}, \quad (5)$$

where $\psi_q = \sqrt{2\pi}(-i)^{(\frac{m}{2}-1)q+1}J_q(\gamma)$. As the diffracted complex amplitude is an explicit function of $\mathcal{R}$, the form of the produced optical pattern remains invariable during propagation.

For a radial phase grating having a sinusoidal profile, by using Eq. (5) the diffraction pattern at a given z can be calculated by $I(r,\theta) = \psi(r,\theta)\psi^*(r,\theta)$, where $*$ denotes a complex conjugate.

In Fig. 1(c) calculated diffraction patterns of three radial phase gratings with different numbers of spokes $m = 10$, $m = 30$, and $m = 50$ are illustrated. The amplitude of the phase modulation for all of the gratings is $\gamma = \pi/2$. In Fig. 1(d) the diffracted phase and intensity distributions from a sinusoidal phase grating with $m = 30$ are shown symmetrically at the left and right sides, respectively. An inset of Fig. 1(d) is shown in Fig. 1(e). The phase distributions are obtained by calculating the quantity $arg[\psi(r,\theta;z)]$ of Eq. (5). The Supplemental Material (SM) Movies 1a and 1b [23] show calculated diffracted intensity and phase patterns for a sinusoidal phase grating with $m = 30$ and $\gamma = \pi/2$ at different propagation distances, respectively. In the calculation of the phase profile during propagation, as in Movie 1b, the term $\exp(ikz)$ of Eq. (5) is not taken into account. Movie 1a shows that the calculated intensity pattern is shape invariant under propagation, and the observed diffraction pattern originates from the center of the grating in the vicinity of $z = 0$. We notice that the phase profiles of Figs. 1(d) and 1(e) and Movie 1b consist of numerous jumps with an absolute value of about π over the azimuthal paths. We call an abrupt phase change with an absolute value of about π a phase anomaly. A more detailed study of the phase anomaly of the light field is presented in a following section. We think that these phase anomalies guarantee an invariant intensity distribution under propagation. Due to the amazing beauty and structural complexity of the resulting patterns we call them "optical carpets."

IV. DIFFRACTION PATTERN OF A RADIAL PHASE GRATING HAVING A BINARY PROFILE

The phase profile induced on a plane wave by a radial phase grating having a binary profile and the number of spokes m [Fig. 1(b)] is given by

$$t(\theta) = e^{i\gamma\,\mathrm{sgn}[\cos(m\theta)]}, \quad (6)$$

where sgn indicates the signum function. The period of $t(\theta)$ is $\frac{2\pi}{m}$, and it can be written in one period by

$$t(\theta) = \begin{cases} e^{i\gamma} & \text{for} \quad \frac{-\pi}{2m} < \theta < \frac{\pi}{2m} \\ e^{-i\gamma} & \text{for} \quad \frac{-\pi}{m} < \theta < \frac{-\pi}{2m} \text{ and } \frac{\pi}{2m} < \theta < \frac{\pi}{m} \end{cases}. \quad (7)$$

By using the above expression one can calculate the Fourier expansion of $t(\theta)$ as follows:

$$t(\theta) = \cos(\gamma) + \sum_{\substack{l=-\infty \\ l\neq 0}}^{\infty} i\,\sin(\gamma) sinc\left(\frac{l\pi}{2}\right)e^{ilm\theta}$$
$$= \cos(\gamma) + \sum_{\substack{l=1 \\ odd}}^{\infty} \frac{2}{l\pi} i^l \sin(\gamma)(e^{ilm\theta} + e^{-ilm\theta}), \quad (8)$$

where $sinc(x) = \frac{\sin(x)}{x}$ and the "odd" under the summation indicates that l is an odd number in the second summation. Moreover, we used the fact that $sinc(\frac{l\pi}{2})$ vanishes for even values of l and it equals to $\frac{2}{l\pi}i^{(l-1)}$ for the odd values of l.

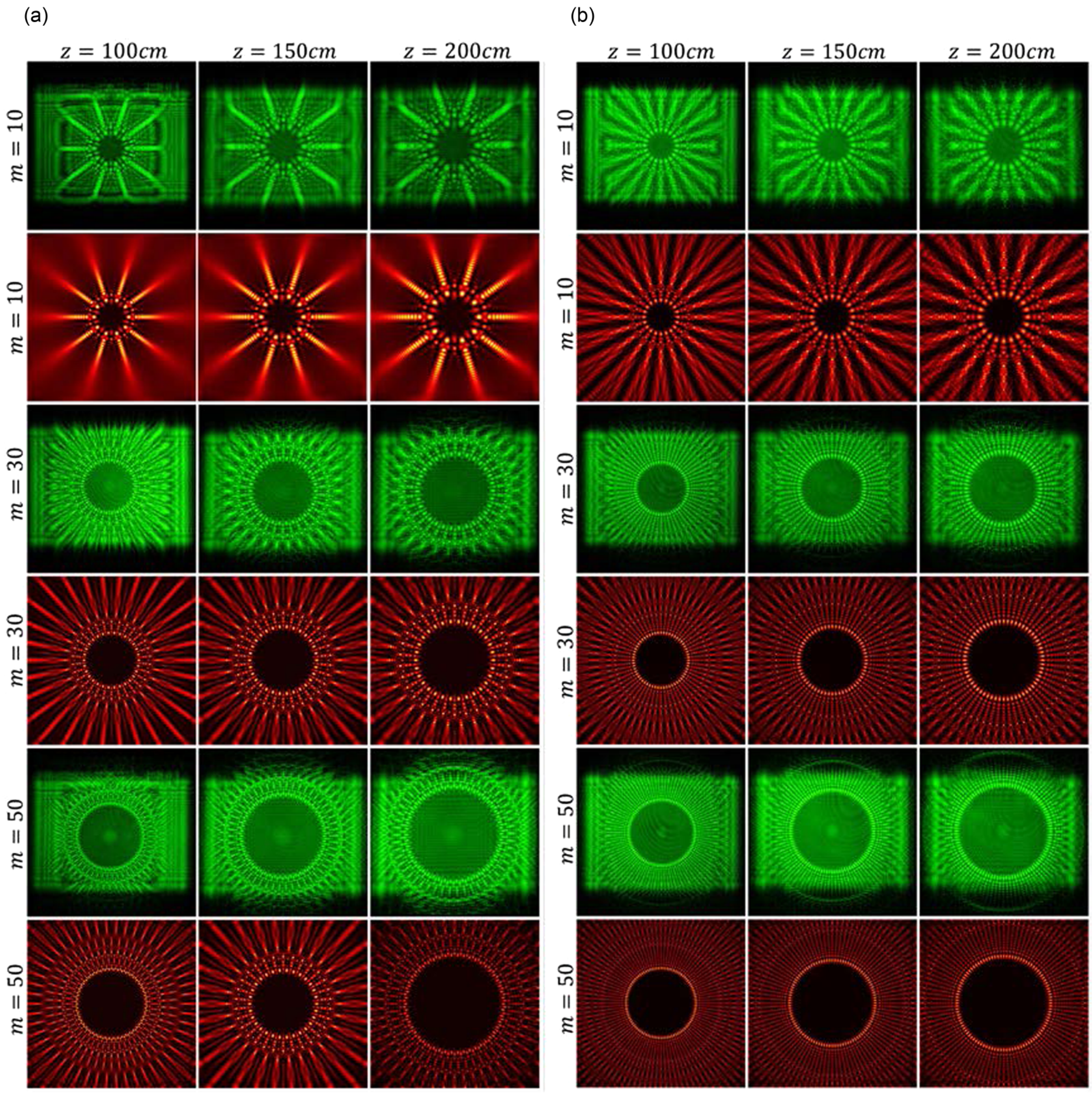

FIG. 2. Shape-invariant carpet beams under propagation, experimentally recorded and simulation results. Simulated and experimentally recorded diffraction patterns from radial phase gratings having (a) sinusoidal and (b) binary profiles, with $m = 10$, $m = 30$, and $m = 50$ spokes at different distances 100 cm, 150 cm, and 200 cm from the structures. The experimentally recorded and simulated patterns are shown by the green and red colors, respectively. The real size of all patterns is 15.6 mm × 15.6 mm. The phase modulation amplitude of the gratings is $\gamma = \pi/2$.

By comparing the second row of Eq. (8) with Eq. (1) one can deduce that $t_0 = \cos(\gamma), t_{n=ml} = t_{n=-ml} = \frac{2}{l\pi} i^l \sin(\gamma), l = 1,3,5,\ldots,$ and all other coefficients are zero. The determined coefficients are replaced in Eq. (2), then the complex amplitude at z is given by

$$\psi(r,\theta;z) = e^{ikz}\left\{\cos(\gamma) + \mathcal{R}e^{i\mathcal{R}^2}\sum_{\substack{l=1\\odd}}^{\infty}\psi_l\left[J_{\frac{lm+1}{2}}(\mathcal{R}^2)\right.\right.$$
$$\left.\left. + i J_{\frac{lm-1}{2}}(\mathcal{R}^2)\right]\cos(lm\theta)\right\}, \quad (9)$$

where $\psi_l = \frac{2}{l}\sqrt{\frac{2}{\pi}}\sin(\gamma)(-i)^{(\frac{m}{2}-1)l+1}$.

Equation (9) specifies the diffracted complex amplitude from a radial phase grating having binary profile. Using Eq. (9), calculated diffraction patterns for three typical binary phase gratings are shown in Fig. 1(f). Calculated phase and intensity patterns for the grating of $m = 30$ with a magnification in size are shown with a mirror symmetry in the left and right sides in Fig. 1(g), respectively. An inset of Fig. 1(g) is shown in Fig. 1(h). The intensity values are normalized to the intensity value of the incident beam. The SM Movies 1c and 1d show calculated diffracted intensity and phase patterns for a binary phase grating with $m = 30$ and $\gamma = \pi/2$ at different z, respectively.

As is illustrated in Figs. 1(g) and 1(h) and seen in Movie 1c, for a binary phase grating when $\gamma = \pi/2$, the number of spokes on the resulting intensity pattern is doubled and equals $2m$, while the spatial period of the phase pattern is still the same period of the grating. This interesting feature stands for all

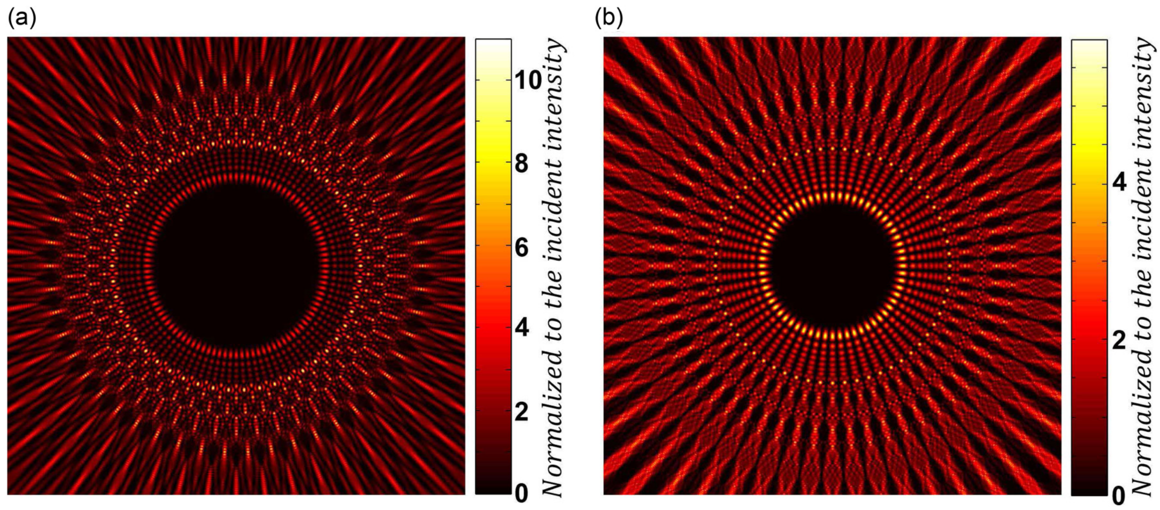

FIG. 3. Calculated intensity profiles for two carpet beams having zero value of intensity in the central area. (a) Calculated intensity of the diffraction pattern from a sinusoidal phase grating with $m = 50$ and $\gamma = 2.4048$ rad at $z = 100$ cm. Here, the intensity of the central area is zero. The real size of the pattern is 15.6 mm × 15.6 mm. (b) The same pattern for a binary phase grating with $\gamma = \pi/2$ and $m = 30$ (see also Movies 2a–2f [23]).

propagation distances. This effect has a beautiful mathematical interpretation. A very close effect also occurs in the near-field diffraction from one-dimensional periodic structures, but only at the quarter-Talbot distances. A detailed mathematical interpretation of this effect was recently presented in Ref. [10].

V. METHODS, SIMULATION, AND EXPERIMENTAL WORKS

In addition to the analytical works, we simulate the diffraction patterns from different radial phase gratings at different propagation distances using the free-space transfer function and MATLAB programming. Also, for a number of radial phase gratings with different spokes the diffraction patterns are experimentally recorded. Movies containing calculated patterns can be found in the Supplemental Material [23].

We used a conventional SLM extracted from a video projector (LCD projector KM3, model no. X50) to prepare the desired pure phase gratings. The maximum amplitude of the phase modulation was limited by $\gamma = \pi/2$, where it was considered in Figs. 1(a) and 1(b). In the experiments, the entire area of the SLMs are fully illuminated by a uniform laser beam. The active area of the SLM is 11 mm × 15 mm, and we have used a square area of 11 mm × 11 mm for producing phase gratings.

In the experiment, a collimated wavefront of the second harmonic of a Nd:YAG diode-pumped laser beam having a wavelength of $\lambda = 532$ nm is propagated through the SLM and the phase grating profile is imposed on it. At different distances from the SLM, we record the diffracted patterns by a camera (Nikon D100). We record the diffraction patterns directly over the active area of the camera by removing the imaging lens of the camera. The active image area of the camera is 23.4 mm × 15.6 mm.

In Fig. 2(a), simulated and experimentally recorded diffraction patterns for three radial sinusoidal phase gratings with different numbers of spokes $m = 10$, $m = 30$, and $m = 50$ are illustrated. In the figure, green and red color patterns correspond to the experimentally recorded and simulated patterns, respectively. The same patterns for three typical radial phase gratings with binary profiles are illustrated in Fig. 2(b).

As can be deduced from Figs. 2(a) and 2(b), the light-field distributions are shape invariant under propagation, and due to the radial symmetry, amazing beauty, and structural complexity of the corresponding intensity patterns, we call the diffracted light beams from the radial phase gratings "radial carpet beams."

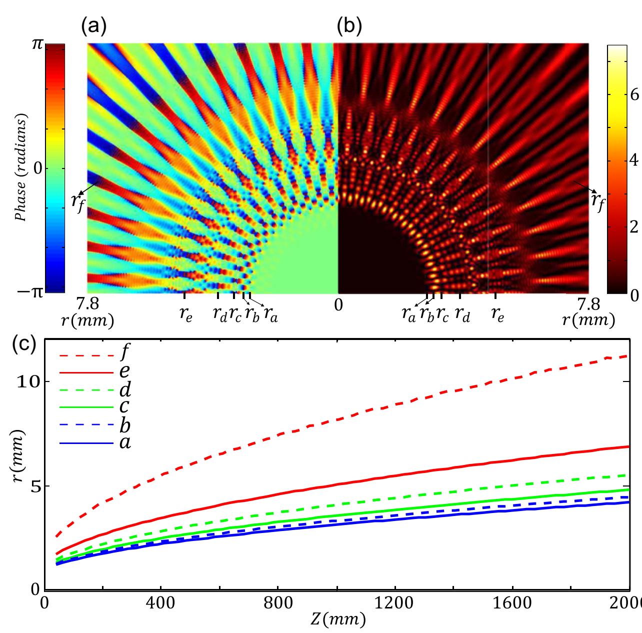

FIG. 4. Self-accelerating property of radial carpet beams. (a, b) Calculated phase and intensity profiles for the diffracted complex light field passing through a sinusoidal phase grating with $m = 50$ and $\gamma = \pi/2$ at $z = 100$ cm. (**c**) Calculated propagation paths for six given intensity rings. Radii of the selected rings at $z = 100$ cm are shown over the first row's profiles.

VI. SPECIFICATION OF THE PRODUCED CARPET PATTERNS AND THE NONDIFFRACTIVE RADIAL CARPET BEAMS

As is apparent from Figs. 1 and 2 over a given transverse plane, three different areas can be recognized. The first area is a "patternless area" that appears in the vicinity of the z axis, and we relate it to the far-field diffraction region. The second area with intermediate radial distances is related to the near-field diffraction region. The area with larger values of the radial coordinates is considered as the geometric shadow. Here the term "shadow" is used for imaging of the phase pattern over the grating. As is apparent from Fig. 1 and from Movies 1a–1d (see SM [23]) the geometric shadow and near-field and far-field diffraction patterns are observable at all transverse planes. This means that the geometric shadow, and the near-field and far-field diffraction regimes, are mixed at various propagation distances. Also, we see that the outer radii of the patternless and near-field diffraction areas increase by propagation. As we have turned a conventional grating into a radial grating with a central singularity, the plane boundaries between the optical regimes are now curved. In other words, similar to the case of amplitude radial gratings, here again the space splits into geometric shadow and far-field and near-field diffraction regimes with nonflat border surfaces (see Fig. 7 of Ref. [19]). Also, it was shown that in the plane-wave diffraction from radial amplitude gratings, in a given transverse plane the realization of the Talbot effect and the conventional Talbot carpet are possible. For more details in this regard and the other aspects of the Talbot carpet at the transverse plane, see Ref. [19].

Unlike the case of diffraction of a plane wave from amplitude radial gratings, here due to a more complicated manipulation of the complex amplitude of the impinging beam by the radial phase gratings, we no longer observe the Talbot effect and are not able to realize it even in the transverse plane.

One of the interesting observations is the nondiffractive behavior of the produced optical carpets. As it is illustrated in Movies 1a and 1c and also in Figs. 2(a) and 2(b), each optical carpet is shape invariant under propagation. Movies 1a and 1c [23] show that the transverse size of the optical carpet at the beginning of the propagation expands rapidly; nevertheless, the rate of expansion decreases by propagation. In the following, we show that unlike the conventional diffraction where the angular form of the far-field diffraction pattern remains unchanged under propagation, here the angular form of the resulting carpets converges by propagation.

As is apparent from Eqs. (5) and (9), the complex amplitude of a carpet beam at a given z is a function of $\mathcal{R}=\sqrt{\frac{\pi}{2\lambda z}}r$; therefore the whole pattern expands with a factor $\sqrt{z}$ during propagation, and the rate of the pattern size increment is $\frac{1}{2\sqrt{z}}$. This rate is a descending function of z. It means that although the size of the pattern increases by a factor $\sqrt{z}$, its angular size decrease by the propagation. This fact reflects the nondiffractive nature of the produced beams. We know that the angular distribution of the far-field diffraction pattern for the convectional apertures remains invariant and the rate of the pattern size increment respect to z is constant [2]. Therefore, the above-mentioned fact is in contradiction with the conventional rules of diffraction optics. The singularity of the radial grating causes this violation from the conventional rules of diffraction optics. As the diffraction of the carpet beams is less than the diffraction of conventional beams such as the Gaussian beams, we have used the nondiffractive term for them.

Another interesting aspect is the focusing of the intensity. As it is shown in Figs. 1(e) and 1(h), the main lobes over each of the calculated diffraction patterns have the maximum value of intensity, with a value about 7 times the intensity of the impinging beam.

Let us present some analytical predictions by considering some approximations of Eq. (5). Similar approximations can be considered for the binary phase gratings using Eq. (9). For large values of $\mathcal{R}$, the Bessel function can be written as [22]

$$J_m(\mathcal{R}^2)\rightarrow\sqrt{\frac{2}{\pi\mathcal{R}^2}}\cos\left(\mathcal{R}^2-\frac{m\pi}{2}-\frac{\pi}{4}\right). \tag{10}$$

Now, for large values of r, by using this approximation, Eq. (5) reduces to

$$\psi(r,\theta;z)=e^{ikz}e^{i\gamma\cos(m\theta')}, \tag{11}$$

which is the geometric shadow of the phase profile of the grating. It means that the phase distribution at large radial distances is the shadow of the phase pattern just after the structure, see Movies 1b and 1d [23].

In the vicinity of the optical axis, when $\mathcal{R}$ goes to zero, by using

$$J_m(\mathcal{R}^2)\rightarrow\frac{1}{\Gamma(m+1)}\left(\frac{\mathcal{R}^2}{2}\right)^m, \tag{12}$$

Eq. (5) reduces to

$$\psi(r,\theta;z)=e^{ikz}\left\{J_0(\gamma)+e^{i\mathcal{R}^2}\sum_{q=1}^{+\infty}\psi_q\mathcal{R}^{qm}\right.$$
$$\left.\times\left[\frac{\mathcal{R}^2+i(qm+1)}{2^{(\frac{qm-1}{2})}(qm+1)\Gamma(\frac{qm+1}{2})}\right]\cos(qm\theta)\right\}. \tag{13}$$

For small values of r, or equally in the vicinity of the optical axis in which $\mathcal{R}<1$, the intensity gets a constant value of $J_0(\gamma)$. An interesting result is obtained when γ is equal to the first zero of J_0, where in this case the intensity of the patternless area is zero. In Fig. 3(a) the carpet pattern for a radial sinusoidal phase grating with $m=50$ and $\gamma=2.4048$ rad at $z=100$ cm is shown. It has a zero value of intensity over the patternless area, and the maximum value of the intensity on the main lobes is about 11 times that of the incident beam intensity. In Fig. 3(b) the carpet pattern of a radial binary phase grating with $m=30$ and $\gamma=\pi/2$ at $z=100$ cm is shown, where the value of intensity over the patternless area is zero. Movies 2a and 2b [23] show the intensity and phase profiles for the carpet beams of sinusoidal phase gratings with $\gamma=\pi/2$ and different values of m at $z=100$ cm, respectively. Movies 2c and 2d show the same profiles for the carpet beams of sinusoidal phase gratings with $\gamma=2.4048$ rad and different values of m at $z=100$ cm, respectively. Movies 2e and 2f show corresponding profiles for the binary phase gratings with $\gamma=\pi/2$ and different values of m at $z=100$ cm, respectively. In fact, each of the resulting beams with a given value of m can be considered as a mode of the carpet beams.

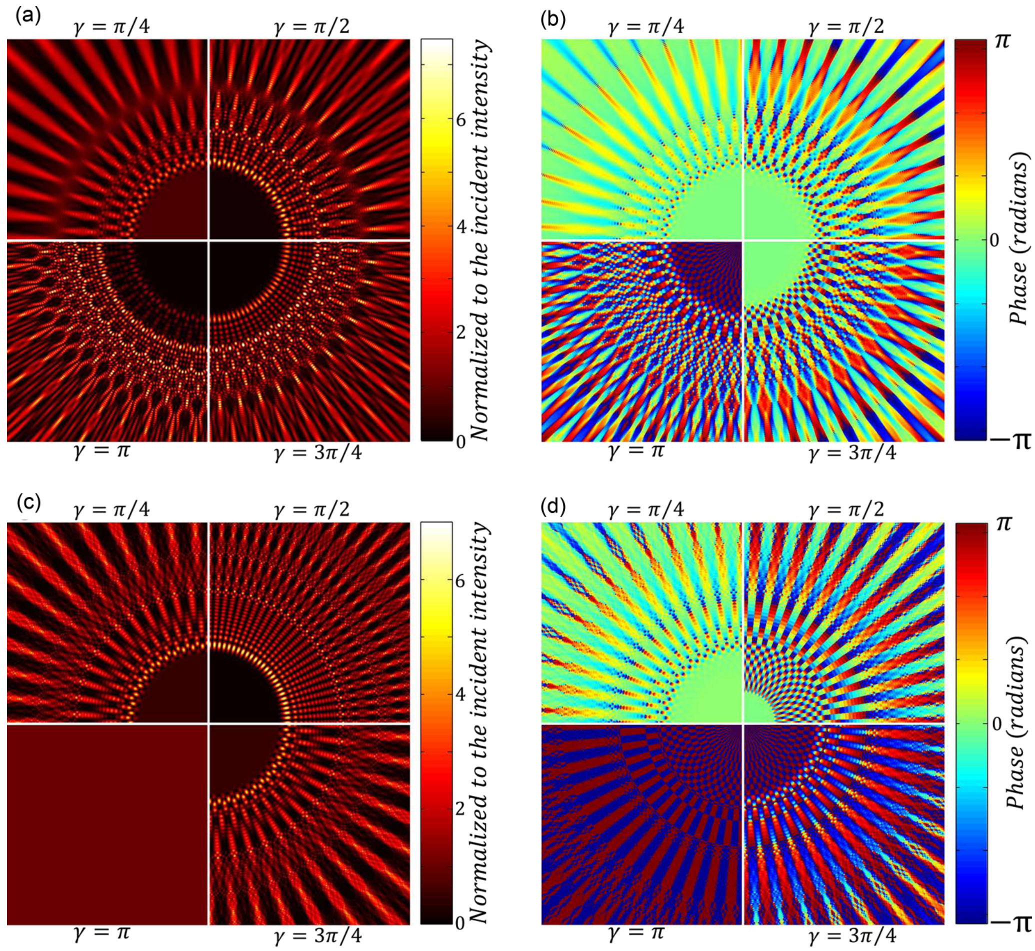

FIG. 5. Architecture of radial carpet beams by tuning the amplitude of phase variation of the grating. (a, b) Calculated intensity and phase distributions of the diffracted field for a sinusoidal phase grating with $m = 50$ and different value of γ at $z = 100$ cm, respectively. (c, d) Show corresponding patterns for a binary phase grating, see also Movies 3a–3d [23].

VII. ACCELERATING SPOT BEAMS

Here, theoretically and experimentally, we show that each part of an optical carpet pattern propagates as an accelerating beam. As is apparent from Fig. 2 and Movies 1a and 1c [23], the form of the carpet patterns remains constant during propagation. Here we show that a given point on the intensity pattern propagates over a curved path.

Equations (5) and (9) show that the diffraction patterns for both sinusoidal and binary cases are explicit functions of $\mathcal{R}$. Therefore, by chasing a given point on the pattern with a given value of $\mathcal{R}$, the trace of the point during propagation can be determined. As $\mathcal{R} = \sqrt{\frac{\pi}{2\lambda z}}r$, for a point on the pattern with a radius of r_0 at a given propagation distance of z_0, its radius r at an arbitrary propagation distance of z can be calculated by $\mathcal{R} = \sqrt{\frac{r_0}{z_0}} = \sqrt{\frac{r}{z}}$, and the trace of the point is given by

$$r(z) = \frac{r_0}{\sqrt{z_0}}\sqrt{z}. \tag{14}$$

This means that the propagation path of a given point on the intensity pattern is a nonstraight line. A similar behavior has been observed for the amplitude radial grating [19].

In Figs. 4(a) and 4(b), quarter parts of the calculated phase and intensity profiles for the diffracted light beam from a sinusoidal phase grating with $m = 50$ and $\gamma = \pi/2$ at $z = 100$ cm are shown, respectively. In Fig. 4(c), calculated paths for six given intensity rings are plotted. Radii of the selected rings at $z = 100$ cm are shown over the patterns of Figs. 4(a) and 4(b). There is a similar self-accelerating behavior for the carpet beams of binary gratings.

VIII. ENGINEERING OF THE CARPET PATTERNS, MODE SELECTION

The physical characteristics of the phase gratings can be easily adjusted to obtain various carpet beams. Here, we investigate some possible ways to achieve different carpet beams that we name "modes." Accessing a large number of modes can be used in different applications such as in optical communications. Also, this feature can be a useful tool in lighting design technologies.

There are different possibilities for mode tuning. Different modes of the carpet beams can be defined and produced through different values of the spoke number m and the phase variation amplitude γ of the phase sinusoidal and binary

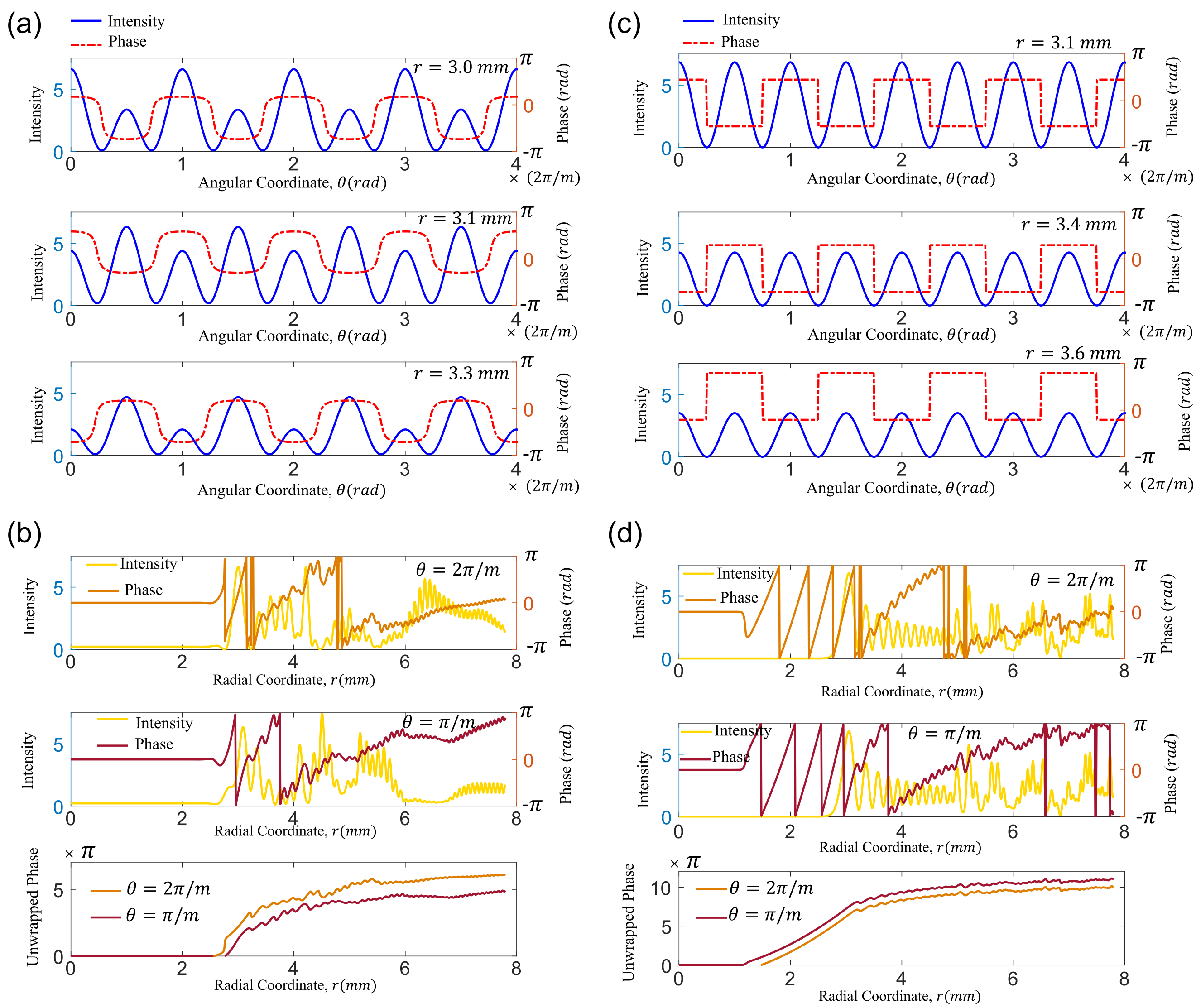

FIG. 6. Phase anomalies of carpet beams. The intensity and phase profiles (a) along three different azimuthal paths and (b) along two different radial paths for the phase pattern of Fig. 5(b) with $\gamma = \pi/2$. Unwrapped phase profiles of (b) are shown in the last row. (c, d) Show corresponding plots for the binary phase grating of Fig. 5(d) with $\gamma = \pi/2$.

gratings. A carpet beam of a radial phase grating, having given values of m and γ, can be considered as a mode of the carpet beams.

Movies 2a and 2b [23] show intensity and phase patterns of successive modes of radial carpet beams generated by tuning the value of m of a sinusoidal phase grating with $\gamma = \pi/2$ at $z = 100$ cm, respectively. Movies 2c and 2d show the same patterns for $\gamma = 2.4048$ rad. Movies 2e and 2f show the same patterns for a binary phase grating with $\gamma = \pi/2$ at $z = 100$ cm.

Now, we show that the form of carpet beams is also sensitive to the value of γ. In Figs. 5(a) and 5(b), calculated diffracted intensity and phase patterns for a sinusoidal phase grating with $m = 50$ at $z = 100$ cm for different values of γ are shown. In Figs. 5(c) and 5(d) the same patterns for a binary phase grating with the same parameters are shown. As is apparent from Figs. 5(a) and 5(c), the forms of intensity patterns are very sensitive to the value of γ. Therefore, another way for defining different modes for the carpet beams can be established by certain values of γ. Movies 3a–3d show the dependency of the intensity and phase distributions to the value of γ for sinusoidal and binary phase gratings. Also, Movies 3a and 3c show that the maximum values of intensities over the main lobes depend on the value of γ.

As the carpet beams are self-healing and are easily switchable through different values of m and γ, they are well-suited for optical communication through atmosphere. Atmospheric turbulence distorts conventional optical beams propagating through it and imposes a major limit in free-space optical communications. By encoding the data on different modes of carpet beams the limit can be bypassed.

IX. PHASE ANOMALIES OF THE PRODUCED LIGHT CARPETS

A well-known phase anomaly for the light field occurs in the passing of a plane wave through a positive lens, on the optical axis in the vicinity of the focal point [24,25]. This interesting

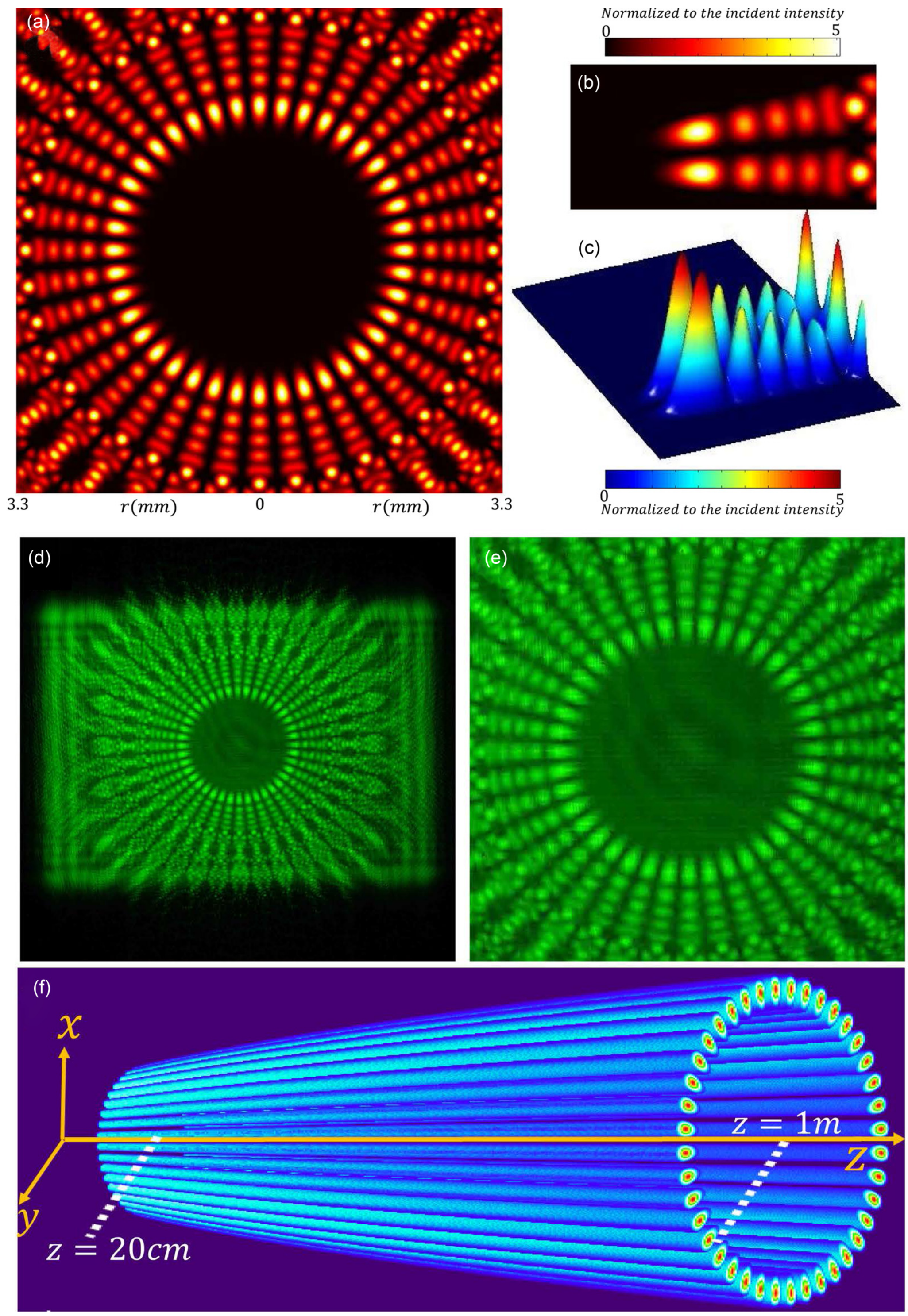

FIG. 7. Radial carpet beams as a 2D optical lattice with a polar symmetry. 2D optical lattice formation by laser beam self-channeling after propagating a plane wave through a radial phase grating with a binary amplitude. (a) Calculated diffraction pattern for a radial phase grating having a binary profile with $m = 20$ spokes at a distance of 100 cm from the grating with a value of $\gamma = \pi/2$. (b, c) Two different illustrations of the intensity profile of a sector of the introduced pattern in (a). (d) An experimentally recorded 2D optical lattice produced by a binary phase grating with the same parameters and at the same distance from the grating of (a). (e) An inset of (d). (f) 3D illustration of the main lobes of (a) under propagation (see also Movie 4 in the Supplemental Material [23]).

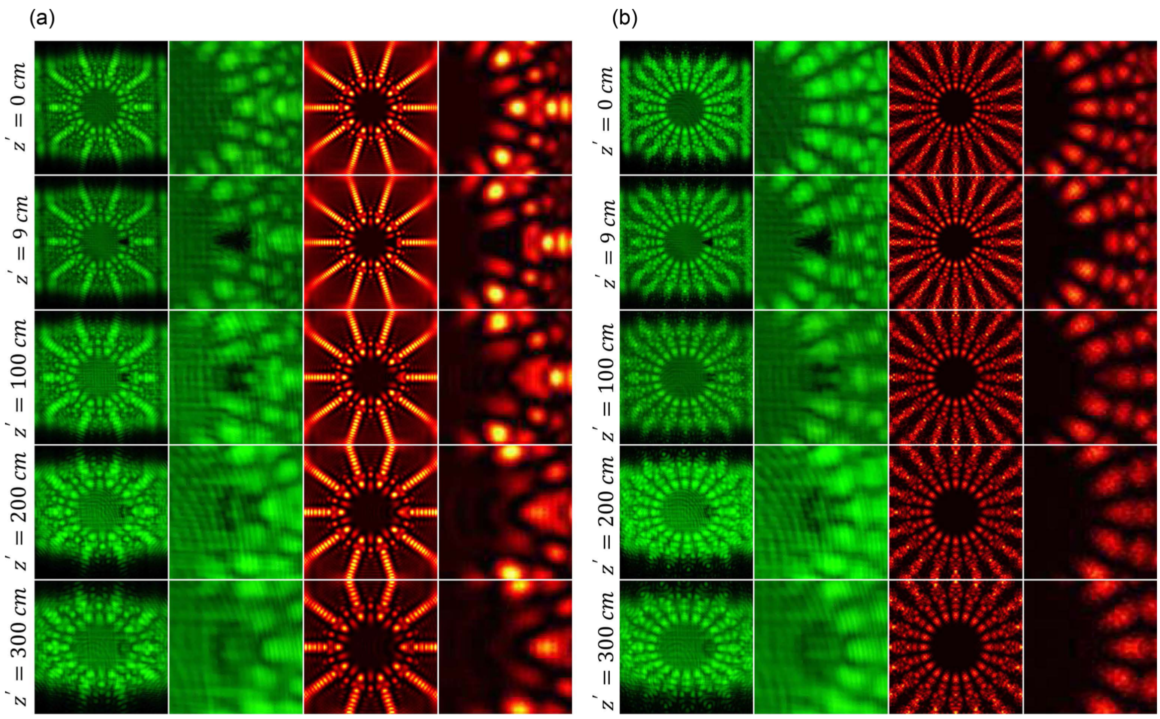

FIG. 8. Self-healing of carpet beams, self-reconstruction of a removed main lobe under propagation. (a) Self-healing of a diffracted beam from a radial phase grating with a sinusoidal profile when one of the main spots is blocked at a distance of $z = 100$ cm from the grating. $z = 100$ cm or equally $z' = 0$ shows the position of the blocking plane. The first and third columns show experimentally observed intensity profiles and the corresponding numerical simulations at different distances from the blocking plane for a radial phase grating having a sinusoidal profile with $m = 10$ spokes and a value of $\gamma = \pi/2$, respectively. The insets of the patterns are maximized in the second and forth columns. The corresponding patterns for a binary phase grating are shown in (b).

feature of the light fields is also observed in the conventional Talbot light carpets [16]. A similar behavior is observed over the phase distributions of the diffracted light fields from the radial gratings. In this section we illustrate this fascinating feature of the carpet beams. The existence of abrupt phase changes for a light field prepares amazing behaviors for the corresponding intensity distribution under propagation. Here, the phase anomaly of the carpet beams is briefly presented.

The phase profile of the diffracted field from a sinusoidal phase grating shown in Fig. 5(b) has a considerable number of phase jumps with an absolute value near π. Also, Movie 3b shows the dependency of the phase anomalies on the value of γ.

In Fig. 6(a), for a sinusoidal phase grating with $m = 50$ and $\gamma = \pi/2$ at $z = 100$ cm, the quantity $arg[\psi(r,\theta;z)]$ of Eq. (5) is plotted in terms of θ at three constant values of r. The corresponding intensity profiles are also plotted for better illustration of the phase jump locations. In Fig. 6(b) the phase and intensity profiles along two radial directions with different values of θ are presented. In the last row, the corresponding unwrapped phase profiles after removing 2π jumps are shown.

In Fig. 6(c) for a binary phase grating with $m = 50$ and $\gamma = \pi/2$ at $z = 100$ cm, the phases of the carpet beam in terms of θ at three different values of r are illustrated. As is apparent from Figs. 6(a) and 6(c) along a given azimuthal path with a constant r, there are phase jumps between all the neighboring intensity lobes. In Fig. 6(d) the phase and intensity profiles along two radial directions with different values of θ for the binary grating are presented. In the last row, the corresponding unwrapped phase profiles after removing 2π jumps are shown. Here, we see that in the azimuthal direction the sinusoidal phase profile of the sinusoidal phase grating shown in Fig. 1(a) by propagation is turned to a binarylike profile, and for the binary phase grating of Fig. 1(b), its binary phase profile is still binary in the azimuthal direction but at different radial distances they do not have the same bias. For both sinusoidal and binary phase gratings, their phase profiles along the radial direction are remarkably changed by propagation, as seen in the last row of Fig. 6.

X. SELF-CHANNELING OF RADIAL CARPET BEAMS, CHARACTERIZATION OF 2D OPTICAL LATTICES

Due to diverse applications of optical lattices in various branches of science, they are attracting great attention. For example, optical lattices are used in the realization of magnetic fields [26], exploration of quantum phase transitions [27], controlling spin-exchange interactions [28], realization of quantum computation [29], and so on. The most simple and early introduced one-dimensional optical lattice is the interference pattern of two coherent beams. Another way for generating optical lattices even in three dimensions (3D) is the use of the self-imaging effect of the 2D periodic structures [11]. By the aid of interference- and diffraction-based methods lattices with limited forms can be produced. In recent years, many optical lattices with a variety of structures have been introduced by the aid of nondiffracting beams, such as the azimuthally modulated

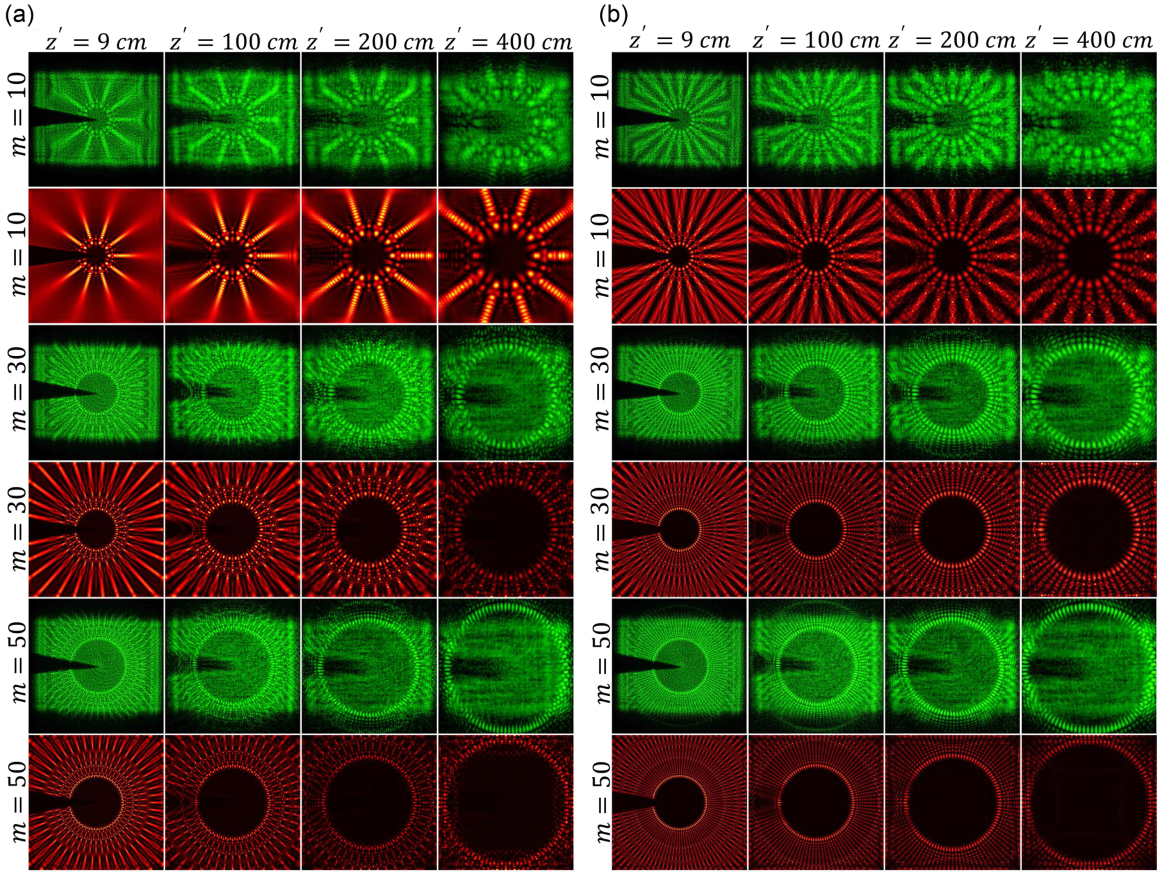

FIG. 9. Self-healing of carpet beams, self-reconstruction of a removed sectoral area under propagation. (a) Green and red color patterns show experimental and simulation results, respectively, at different distances from the blocking plane, $z' = 0$, for three sinusoidal phase gratings with $m = 10$, $m = 30$, and $m = 50$ and $\gamma = \pi/2$. The corresponding patterns for binary phase gratings are shown in (b).

Bessel and circular Airy beams, and combination of parabolic beams [21,30–32].

It is worth mentioning that the laser beam channeling also occurs by the filamentation of ultraintense laser pulses in transparent dielectrics [18,33,34], where the formation of filaments results by the dynamic balance between various linear and nonlinear processes.

Optical lattice are also formed by the interference of two light beams on materials showing nonlinear refractive index dependency on light intensity. These photonic lattices have been extensively discussed, since they can be erased and controlled by the beam properties [35].

Unlike filamentation of the conventional laser beams that occurs only in transparent media [34], self-channeling of nondiffracting beams may well occur even in free space. For a radial carpet beam we showed that there are numerous phase anomalies over the diffracted beam in the azimuthal direction at all propagation distances. These phase anomalies provide a self-channeling property for the light beam under propagation.

In this section, formation of a 2D optical lattice by laser beam self-channeling in the propagation of a plane wave through a binary phase grating is investigated. Self-channeling of the diffracted beam is investigated both via computer simulation and experimental work. These lattices are very easily tunable by changing the values of m and γ of the grating. We believe that this kind of 2D optical lattices can be very useful for the lensless laser patterning and laser manipulation techniques, light-sheet microscopy, controllable generating of multiple filament plasma channels in the field of plasma physics, etc.

In Fig. 7(a), formation of a 2D optical lattice by propagation of a plane wave through a binary phase grating having $m = 20$ and $\gamma = \pi/2$ at $z = 100$ cm is illustrated. Figures 7(b) and 7(c) show the intensity profile over a sector of Fig. 7(a) by two different ways. Figure 7(d) shows an experimentally recorded 2D optical lattice produced by the same grating at the same propagation distance. In Fig. 7(e) an inset of Fig. 7(d) is shown. Figure 7(f) illustrates the 3D form of the central lobes of a given radial carpet beam produced by the same grating.

As it is seen from Fig. 7(f), the transverse size of the main lobes is almost constant during propagation. The SM Movies 4a–4d show shape-invariant behaviors of the carpet patterns of sinusoidal and binary phase gratings during propagation from $z = 2\,m$ to $z = 3\,m$. Movie 4c shows that the radial dimensions of the patternless area at $z = 2\,m$ and $z = 3\,m$ are 2.2 mm and 2.35 mm, respectively. This means that the radial dimension of the carpet beam in that range increases 6 %. For large values of propagation distances, this percentage of the size increases towards to zero.

It is worth noting that there is an increasing interest in understanding the nonlinear propagation of accelerating beams, e.g., Airy beams [36]. The beam properties and propagation can

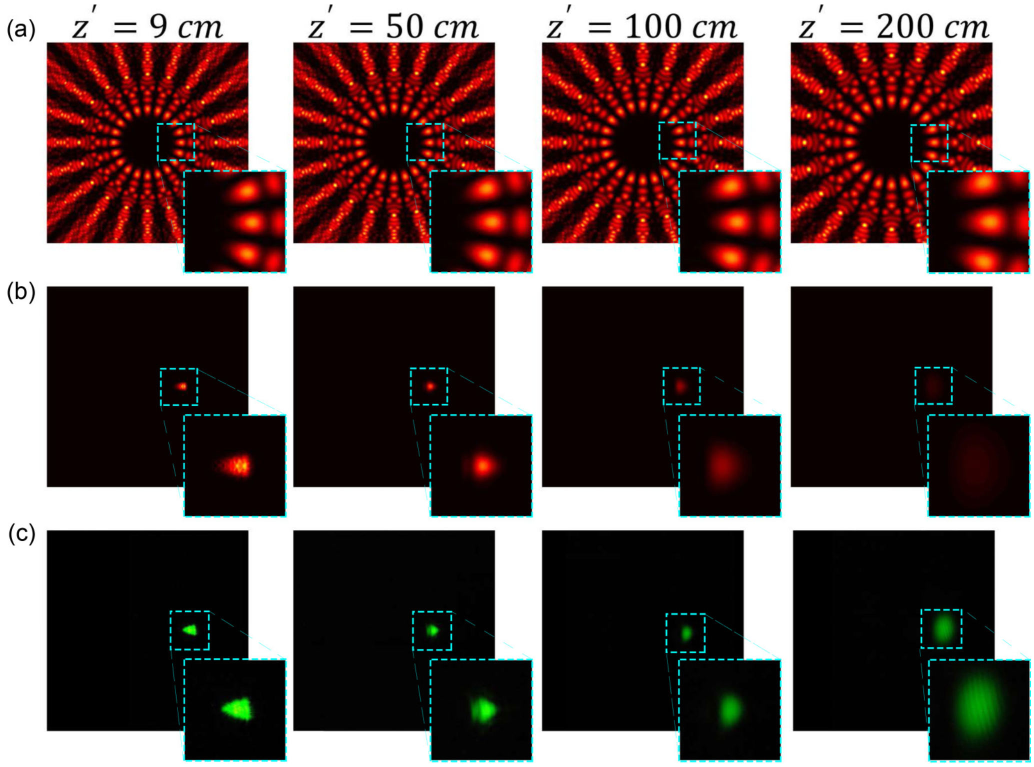

FIG. 10. Effect of an exaggerated cancellation on the self-healing and nondiffracting properties of the carpet beams. (a) Illustration of the entire beam propagation. Insets show enlarged intensity profiles of three main lobes at different propagation distances. (b) Simulated and (c) experimentally recorded intensity profiles at different distances from a suitable mask, z', where a main lobe is isolated by passing through the mask installed at distance $z = 300$ cm from a binary phase grating. Insets again show enlarged intensity profiles of the main lobe at different propagation distances.

be modified by the nonlinear light-matter interactions, such as the light self-focusing that leads to the formation of spatial soliton. In the case of radial carpet beams, such study may show some specific properties of these beams under nonlinear propagation.

XI. SELF-HEALING PROPERTIES OF THE PRODUCED OPTICAL BEAMS

Here, we investigate both by numerical simulation and experimental observation the self-healing properties of the produced optical carpet beams. We show that this kind of beam tends to reform during propagation in spite of the severity of the imposed perturbations. We investigate this behavior by blocking one of the main spots of the beams and by blocking a sectoral area of the beams. Our observations are in excellent agreement with the numerical simulations.

In addition, we investigate the effect of m and γ of the phase grating on the self-healing and autofocusing properties of the beams. We show that for larger value of m and $\gamma = \pi/2$ the self-healing is efficient.

In Figs. 8(a) and 8(b), self-healing of a diffracted beam is illustrated when one of the main lobes is blocked at a distance of 100 cm from two gratings with sinusoidal and binary phase profiles, respectively. In Figs. 9(a) and 9(b), self-healing of a diffracted beam is shown where a sectoral area is blocked at a distance of 100 cm from two gratings with sinusoidal and binary phase profiles, respectively. As is apparent from Figs. 8 and 9, there is a good agreement between results of experimental observations and numerical simulations.

Now let us examine the effect of an exaggerated cancellation on the self-healing and nondiffracting properties of the carpet beams. For this purpose, one of the main lobes is isolated with a suitable mask installed at a given distance from the grating. For better comparing propagation of the isolated lobe with the case where it propagates with the whole beam, in Fig. 10(a), the intensity profiles of the whole beam at different propagation distances are shown, and in the insets three central main lobes are enlarged. As is apparent, because these lobes propagate with the whole beam, their sizes and intensity profiles are invariant under propagation. In Fig. 10(b), transformation of an isolated main lobe at different propagation distances from the mask is simulated, where the mask is installed at a distance of $z = 300$ cm from the grating. Corresponding experimental results are shown in Fig. 10(c). In Figs. 10(b) and 10(c), the insets show the intensity distribution of the main lobe with a magnification in size at different propagation distances. Both simulated and experimental results show that a lobe diverges very rapidly when it propagates alone.

The above-presented experimental works and simulated results of the self-healing behavior of the radial carpet beams indicate that there are transverse energy flows between the individual light structures as propagation increases. The self-reconstruction or self-healing of the produced beams can be interpreted through their possible internal transverse power flow. The same result can also be deduced due to the curved light trajectories of the beams. Further considerations in this regard need to take into account a detailed study on the Poynting vector of the beams, and calculate the transverse components of the phase gradients of the light beam under propagation. Theoretical investigation of the observed self-healing properties and the robustness of these optical patterns in scattering and turbulent environments are under study. Similar self-healing properties were previously observed for the other kind of nondiffractive beams such as the Airy beams [12].

XII. CONCLUSION

A class of accelerating and self-healing light beams was produced by diffraction of a plane wave from radial phase gratings. Unprecedented optical carpets at the transverse plane and tunable 2D optical lattices in the polar coordinates were observed. The name "carpet" stands for the peculiar intensity profiles of the generated beams. We believe that these beautiful optical carpets and optical lattices have led to exciting new applications and many intriguing ideas. We think that radial carpet beams are a class of direct solution of the Maxwell equations. This theoretical work is under study. We also think that the same carpet beams can be generated and amplified directly by a laser source if the same radial constraints are imposed on the mirrors of the laser cavity. Investigation of the nonlinear propagation of radial carpet beams is another interesting study. Finally, the fusion of the diffraction properties of the radial gratings with singular optics is an interesting subject. Although we have recently presented some interesting results of the diffraction of vortex beams from conventional radial amplitude gratings [20], the diffraction of a vortex beam from phase radial gratings and the diffraction of vortex beams from radial gratings, having any additional out-of-center singularities [37,38], are under study.

ACKNOWLEDGMENTS

S.R. acknowledges support from the IASBS Research Council under Grants No. G2016IASBS12632 and No. G2017IASBS12632.

S.R. designed the research. A.M.K. and S.R. performed the experiments. All authors contributed to the simulations. D.H. and S.R. performed theoretical works. S.R. performed analysis and interpretation of the results. S.R. drafted the manuscript.

[1] N. Marsal, D. Wolfersberger, M. Sciamanna, and G. Montemezzani, Noise- and dynamics-sustained patterns in a nonlinear photorefractive system, Phys. Rev. A **81**, 031804 (2010).

[2] S. A. Akhmanov and S. Y. Nikitin, *Physical Optics* (Oxford University Press, New York, 1997).

[3] Z. Bouchal and M. Olivík, Non-diffractive vector Bessel beams, J. Mod. Opt. **42**, 1555 (1995).

[4] M. V. Berry and N. L. Balazs, Nonspreading wave packets, Am. J. Phys. **47**, 264 (1979).

[5] G. A. Siviloglou, J. Broky, A. Dogariu, and D. N. Christodoulides, Observation of Accelerating Airy Beams, Phys. Rev. Lett. **99**, 213901 (2007).

[6] J. C. Gutierrez-Vega, M. D. Iturbe-Castillo, and S. Chavez-Cerda, Alternative formulation for invariant optical fields: Mathieu beams, Opt. Lett. **25**, 1493 (2000).

[7] P. Zhang, Y. Hu, T. Li, D. Cannan, X. Yin, R. Morandotti, Z. Chen, and X. Zhang, Nonparaxial Mathieu and Weber Accelerating Beams, Phys. Rev. Lett. **109**, 193901 (2012).

[8] J. D. Ring, J. Lindberg, A. Mourka, M. Mazilu, K. Dholakia, and M. R. Dennis, Auto-focusing and self-healing of Pearcey beams, Opt. Express **20**, 18955 (2012).

[9] J. Wen, Y. Zhang, and M. Xiao, The Talbot effect: recent advances in classical optics, nonlinear optics, and quantum optics, Adv. Opt. Photonics **5**, 83 (2013).

[10] S. Rasouli and D. Hebri, Contrast enhanced quarter-Talbot images, J. Opt. Soc. Am. A **34**, 2145 (2017).

[11] S. Rasouli, D. Hebri, and A. M. Khazaei, Investigation of various behaviors of near- and far-field diffractions from multiplicatively separable structures in the x and y directions, and a detailed study of the near-field diffraction patterns of 2D multiplicatively separable periodic structures using the contrast variation method, J. Opt. **19**, 095601 (2017).

[12] J. Broky, G. A. Siviloglou, A. Dogariu, and D. N. Christodoulides, Self-healing properties of optical Airy beams, Opt. Express **16**, 12880 (2008).

[13] F. Diebel, M. Boguslawski, T. Dadalyan, R. Drampyan, and C. Denz, Controlled soliton formation in tailored Bessel photonic lattices, Opt. Express **24**, 12933 (2016).

[14] X. Pang, G. Gbur, and T. D. Visser, The Gouy phase of Airy beams, Opt. Lett. **36**, 2492 (2011).

[15] M. S. Kim, T. Scharf, A. da Costa Assafrao, C. Rockstuhl, S. F. Pereira, H. P. Urbach, and H. P. Herzig, Phase anomalies in Bessel-Gauss beams, Opt. Express **20**, 28929 (2012).

[16] M.-S. Kim, T. Scharf, C. Menzel, C. Rockstuhl, and H. P. Herzig, Phase anomalies in Talbot light carpets of self-images, Opt. Express **21**, 1287 (2013).

[17] I. Kaminer, M. Segev, and D. N. Christodoulides, Self-Accelerating Self-Trapped Optical Beams, Phys. Rev. Lett. **106**, 213903 (2011).

[18] M. A. Bandres, I. Kaminer, M. Mills, B. M. Rodríguez-Lara, E. Greenfield, M. Segev, and D. N. Christodoulides, Accelerating optical beams, Opt. Photonics News **24**, 30 (2013).

[19] S. Rasouli, A. M. Khazaei, and D. Hebri, Talbot carpet at the transverse plane produced in the diffraction of plane wave from amplitude radial gratings, J. Opt. Soc. Am. A **35**, 55 (2018).

[20] D. Hebri, S. Rasouli, and M. Yeganeh, Intensity-based measuring of the topological charge alteration by the diffraction of vortex beams from amplitude sinusoidal radial gratings, J. Opt. Soc. Am. B **35**, 724 (2018).

[21] A. P. Porfirev and S. N. Khonina, Generation of azimuthally modulated circular superlinear Airy beams, J. Opt. Soc. Am. B **34**, 2544 (2017).

[22] G. B. Arfken, *Mathematical Methods for Physicists*, 3rd ed. (Academic Press, New York, 1985).

[23] See Supplemental Material at http://link.aps.org/supplemental/10.1103/PhysRevA.97.033844 for movies showing calculated diffracted intensity and phase patterns for a sinusoidal or a binary phase grating as a function of z, m, or γ.
[24] S. Feng and H. G. Winful, Physical origin of the Gouy phase shift, Opt. Lett. **26**, 485 (2001).
[25] M. S. Kim, A. Naqavi, T. Scharf, K. J. Weible, R. Volkel, C. Rockstuhl, and H. P. Herzig, Experimental and theoretical study of the Gouy phase anomaly of light in the focus of microlenses, J. Opt. **15**, 105708 (2013).
[26] M. Aidelsburger, M. Atala, S. Nascimbene, S. Trotzky, Y. A. Chen, and I. Bloch, Experimental Realization of Strong Effective Magnetic Fields in an Optical Lattice, Phys. Rev. Lett. **107**, 255301 (2011).
[27] I. Bloch, J. Dalibard, and S. Nascimbene, Quantum simulations with ultracold quantum gases, Nat. Phys. **8**, 267 (2012).
[28] L. M. Duan, E. Demler, and M. D. Lukin, Controlling Spin Exchange Interactions of Ultracold Atoms in Optical Lattices, Phys. Rev. Lett. **91**, 090402 (2003).
[29] G. K. Brennen, C. M. Caves, P. S. Jessen, and I. H. Deutsch, Quantum Logic Gates in Optical Lattices, Phys. Rev. Lett. **82**, 1060 (1999).
[30] P. Rose, M. Boguslawski, and C. Denz, Nonlinear lattice structures based on families of complex nondiffracting beams, New J. Phys. **14**, 033018 (2012).
[31] J. S. Rodrigues, C. V. C. Mendes, E. J. S. Fonseca, A. J. Jesus-Silva, Talbot effect in optical lattices with topological charge, Opt. Lett. **42**, 3944 (2017).
[32] Y. V. Kartashov, V. A. Vysloukh, and L. Torner, Soliton shape and mobility control in optical lattices, Prog. Opt. **52**, 63 (2009).
[33] P. Polynkin, M. Kolesik, and J. Moloney, Filamentation of Femtosecond Laser Airy Beams in Water, Phys. Rev. Lett. **103**, 123902 (2009).
[34] A. Couairon and A. Mysyrowicz, Femtosecond filamentation in transparent media, Phys. Rep. **441**, 47 (2007).
[35] A. A. Sukhorukov, N. Marsal, A. Minovich, D. Wolfersberger, M. Sciamanna, G. Montemezzani, and D. N. Neshev, Lattice-controlled modulation instability in photorefractive feedback systems, Opt. Lett. **35**, 3568 (2010).
[36] N. Wiersma, N. Marsal, M. Sciamanna, and D. Wolfersberger, Airy beam self-focusing in a photorefractive medium, Sci. Rep. **6**, 35078 (2016).
[37] S. Rasouli and M. Yeganeh, Formulation of the moiré patterns formed by superimposing of gratings consisting of topological defects: Moiré technique as a tool in singular optics detections, J. Opt. **17**, 105604 (2015).
[38] M. Yeganeh and S. Rasouli, Investigation of the moiré patterns of defected radial and circular gratings using the reciprocal vectors approach, J. Opt. Soc. Am. A **33**, 416 (2016).